Brief Report

Stroke and Neurodegeneration Induce Different Connectivity Aberrations in the Insula

Indira García-Cordero, PhD; Lucas Sedeño, PhD; Daniel Fraiman, PhD; Damian Craiem, PhD; Laura Alethia de la Fuente, MSc; Paula Salamone, PhD; Cecilia Serrano, MD; Luciano Sposato, PhD; Facundo Manes, PhD; Agustín Ibañez, PhD

Background and Purpose—Stroke and neurodegeneration cause significant brain damage and cognitive impairment, especially if the insular cortex is compromised. This study explores for the first time whether these 2 causes differentially alter connectivity patterns in the insular cortex.

Methods—Resting state–functional magnetic resonance imaging data were collected from patients with insular stroke, patients with behavioral variant frontotemporal dementia, and healthy controls. Data from the 3 groups were assessed through a correlation function analysis. Specifically, we compared decreases in connectivity as a function of voxel Euclidean distance within the insular cortex.

Results—Relative to controls, patients with stroke showed faster connectivity decays as a function of distance (hypoconnectivity). In contrast, the behavioral variant frontotemporal dementia group exhibited significant hyperconnectivity between neighboring voxels. Both patient groups evinced global hypoconnectivity. No between-group differences were observed in a volumetrically and functionally comparable region without ischemia or neurodegeneration.

Conclusions—Functional insular cortex connectivity is affected differently by cerebral ischemia and neurodegeneration, possibly because of differences in the cause-specific pathophysiological mechanisms of each disease. These findings have important clinical and theoretical implications. **(*Stroke*. 2015;46:00-00. DOI: 10.1161/STROKEAHA.115.009598.)**

Key Words: cerebral cortex ■ dementia ■ magnetic resonance imaging ■ stroke

The insular cortex (InsC) is a main structural–functional hub of the brain.[1] It features widespread connections with cortical and subcortical regions, and it is implicated in varied domains, such as body sensation, language, emotion, and social cognition.[2] Notably, the InsC abounds in von Economo neurons, which facilitate rapid integration of information. Together with its topological centrality,[1] these features render the InsC as a core region for overall brain dynamics and cognition.

InsC damage after stroke or neurodegeneration can considerably impair cognitive function. Stroke can disturb behavioral, emotional, and sensory domains,[3] whereas early neurodegeneration (including the InsC) in behavioral variant frontotemporal dementia (bvFTD)[4] usually leads to social and emotional dysfunction.[5] Despite such general differences, little is known about the distinct insular connectivity alterations caused by each of these causes. A direct comparison of InsC connectivity patterns in patients affected by stroke and neurodegeneration[6] may reveal theoretically and clinically relevant differences between each pathophysiological process.

In fact, at the molecular level, these conditions differ in timing and physiopathology. Stroke involves tissue loss, neuronal reorganization, and plasticity.[7] Instead, neurodegeneration in bvFTD results from protein aggregation, inducing physiopathological events (eg, axonal degeneration, synapse loss, and dendritic retraction) and propagation of misfolded proteins.[8] These differences at the molecular level suggest that InsC connectivity may be differentially affected by stroke and bvFTD.

Previous studies have reported aberrant long-range connectivity (mostly hypoconnectivity) in both stroke and bvFTD.[4,7] Nevertheless, local connectivity is a key feature

Received April 1, 2015; final revision received May 22, 2015; accepted June 11, 2015.

From the Laboratory of Experimental Psychology and Neuroscience (LPEN), Institute of Cognitive Neurology (INECO), Favaloro University, Buenos Aires, Argentina (I.G.-G., L.S., L.A.d.l.F., P.S., F.M., A.I.); UDP-INECO Foundation Core on Neuroscience (UIFCoN), Faculty of Psychology, Diego Portales University, Santiago, Chile (L.S., F.M., A.I.); National Scientific and Technical Research Council (CONICET), Buenos Aires, Argentina (L.S., D.F., D.C., F.M., A.I.); Laboratorio de Investigación en Neurociencia, Universidad de San Andrés, Buenos Aires, Argentina (D.F.); Facultad de Ingeniería, Ciencias Exactas y Naturales, Universidad Favaloro, Buenos Aires, Argentina (D.C.); Memory and Balance Clinic, Buenos Aires, Argentina (C.S.); Department of Clinical Neurological Sciences, Western University, London, Canada (L.S.); Universidad Autónoma del Caribe, Barranquilla, Colombia (A.I.); and ACR Centre of Excellence in Cognition and its Disorders, Sydney, Australia (F.M., A.I.).

Guest Editor for this article was Sean Savitz, MD.

The online-only Data Supplement is available with this article at http://stroke.ahajournals.org/lookup/suppl/doi:10.1161/STROKEAHA.115.009598/-/DC1.

Correspondence to Agustín Ibáñez, PhD, Institute of Cognitive Neurology and Neuroscience, Pacheco de Melo 1860, Buenos Aires, C1126AAB, Argentina. E-mail aibanez@ineco.org.ar

of brain dynamics.[9] Unlike global connectivity (which may be similarly altered across pathologies), this dimension may better discriminate between diseases. Crucially, it modulates global connectivity[10] and is fundamental for the emergence of small-world properties. Yet, local connectivity research has been rather sparse in neurological populations, especially in patients with stroke. In neurodegeneration, local connectivity disturbances may constitute a key disease marker[9] and a useful dimension to characterize regions of early atrophy. Thus, our focus is on local connectivity because the InsC in consistently compromised in both groups.

To address this hitherto unexplored issue, we assessed InsC functional connectivity in patients with stroke and bvFTD. Specifically, we focused on correlations between local connectivity decays and intervoxel distance within the InsC. By considering various spatial ranges in connectivity, we aimed to reveal cause-specific patterns of regional functional connectivity of InsC at both small and large levels.

Methods

We recruited 33 participants from an ongoing project.[6] The sample comprised 1 patient with hemorrhagic and 7 patients with ischemic stroke, all featuring damage to the InsC and also peripheral areas (38–66 years, 2 women: 6 men, Mini-Mental State Examination: 29 [26–30]; Figure A; Table I in the online-only Data Supplement), 11 patients with probable bvFTD (54–70 years, 6 women: 5 men, Mini-Mental State Examination: 25.11 [18–30]; Figure B), and 14 healthy subjects (33–72, 4 women: 10 men, Mini-Mental State Examination: 29.23 [25–30]; Section 1.1 in the online-only Data Supplement). The 3 groups were matched by age, sex, educational level, and premorbid intelligence quotient. All participants provided signed consent in accordance with the Declaration of Helsinki. The study was approved by the Ethics Committee of the Institute of Cognitive Neurology.

Structural images and resting functional magnetic resonance imaging were acquired from patients and healthy subjects in a-1.5 T Phillips Intera scanner (Section 1.2.1 in the online-only Data Supplement). Demographic information was compared among groups using ANOVAs and Pearson χ^2 tests. The global atrophy pattern in patients with bvFTD was assessed through voxel-based morphometry (Figure B; Section 1.2.3 in the online-only Data Supplement). Functional images were slice-time corrected, realigned, and normalized on SPM8. They were subsequently band-pass filtered (0.01–0.05 Hz). We finally regressed out the 6 motion parameters estimated during realignment (Section 1.2.4 in the online-only Data Supplement). All groups were also compared in terms of long-range connectivity between InsC and regions of interest (ROIs) of 6 functionally defined networks (Section 1.2.5 in the online-only Data Supplement).

Correlation Function

We assessed local InsC connectivity by analyzing interaction decays as a function of between-voxel distance. This approach is similar to previously reported regional homogeneity analyses,[11] as both assess local correlations. However, the distance measure in regional homogeneity analyses is a fixed point rather than a dimensional parameter, and distant correlations are not even considered within a region. The correlation function analysis allowed us to study the interaction between voxels which are at a distance d (for all possible values of d), assessing connectivity variations within the InsC at different levels: at the small spatial level, we analyzed voxels in close proximity; at the large spatial level, we studied distant regional connectivity among InsC voxels. The level of functional decay indicates whether local connectivity in a ROI is affected by disease.

Blood oxygen level–dependent contrast imaging temporal series and x–y–z coordinates in Montreal Neurological Institute space were calculated for each voxel in 2 bilateral ROIs: the InsC and the cuneus (as defined in the automated anatomical label atlas). The cuneus was selected as a control area because it resembles the insula's size and functional properties (viz, integration of sensory and high-order information), but it was not affected by bvFTD atrophy or stroke in our patients (Figure A and B).

We determined the degree of functional interaction between voxels lying at a distance d within each ROI. To this end, we calculated the average Spearman rank correlation coefficient, ρ, between blood oxygen level–dependent contrast imaging signals of voxels separated by d. We studied this measure (henceforth, correlation function) as a function of the Euclidean distance (d) between voxels, as follows:

$$\rho(d) = \frac{1}{\#V_d} \sum_{(i,j)\in V_d} r_{ij},$$

where $V_d = \{(i,j) \text{voxels} \in \text{ROI: dist}(i,j) = d\}$,

$r_{ij} = 1 - \frac{6}{T(T^2-1)} \sum_{t=1}^{T} \left(\tilde{B}_i(t) - \tilde{B}_j(t)\right)^2$, $\tilde{B}_k(t)$ is the rank time series of the blood oxygen level–dependent contrast imaging signal of the k voxel, and T is the length of this signal.

This function was calculated for each subject and ROI and averaged within groups (Section 1.2.6 in the online-only Data Supplement).

Correlation functions were compared via Monte Carlo permutation tests combined with bootstrapping (Section 1.2.6 in the online-only Data Supplement). This simple method gives a straightforward solution for the multiple comparison problems and does not depend on multiple comparison corrections or Gaussian distribution assumptions.

Results

The groups presented no significant differences in sex, age, formal education, or premorbid intelligence quotient (Table).

Figure A shows the lesion overlap of the InsC, which was the most consistently affected region across patients (Table I in the online-only Data Supplement). Voxel-based morphometry analysis revealed a pattern of global atrophy in the bvFTD group in fronto-temporo-insular structures (P<0.05; false discovery rate corrected; Figure B), which replicated previous reports[4] (Section 2.2 and Table II in the online-only Data Supplement). We have also provided global volumetric measures (grey matter, white matter, and cerebrospinal fluid) of patients with bvFTD and controls (Sections 1.2.3 and 2.2 and Table III in the online-only Data Supplement).

Grey matter volume of intact/infarcted/atrophied InsC for both patient groups is described in Tables IV and V in the online-only Data Supplement (Methods Section 1.2.3 and Extended Results Section 2.2 in the online-only Data Supplement). To control for possible InsC differences among patient groups, we compared the extent of bilateral insular damage induced by stroke and bvFTD atrophy. The number of infarcted versus atrophic voxels and the volume of infarcted versus atrophied areas were comparable in both groups (Section 1.2.7 in the online-only Data Supplement).

For patients with stroke, when compared with controls, pairwise correlations between long-range voxels within bilateral InsCs significantly decreased as a function of voxel distance (P<0.05). Such hypoconnectivity appeared at a distance of ≈9 to 19 voxels (18–40 mm; Figure C). Conversely, patients with bvFTD, relative to controls, showed significant

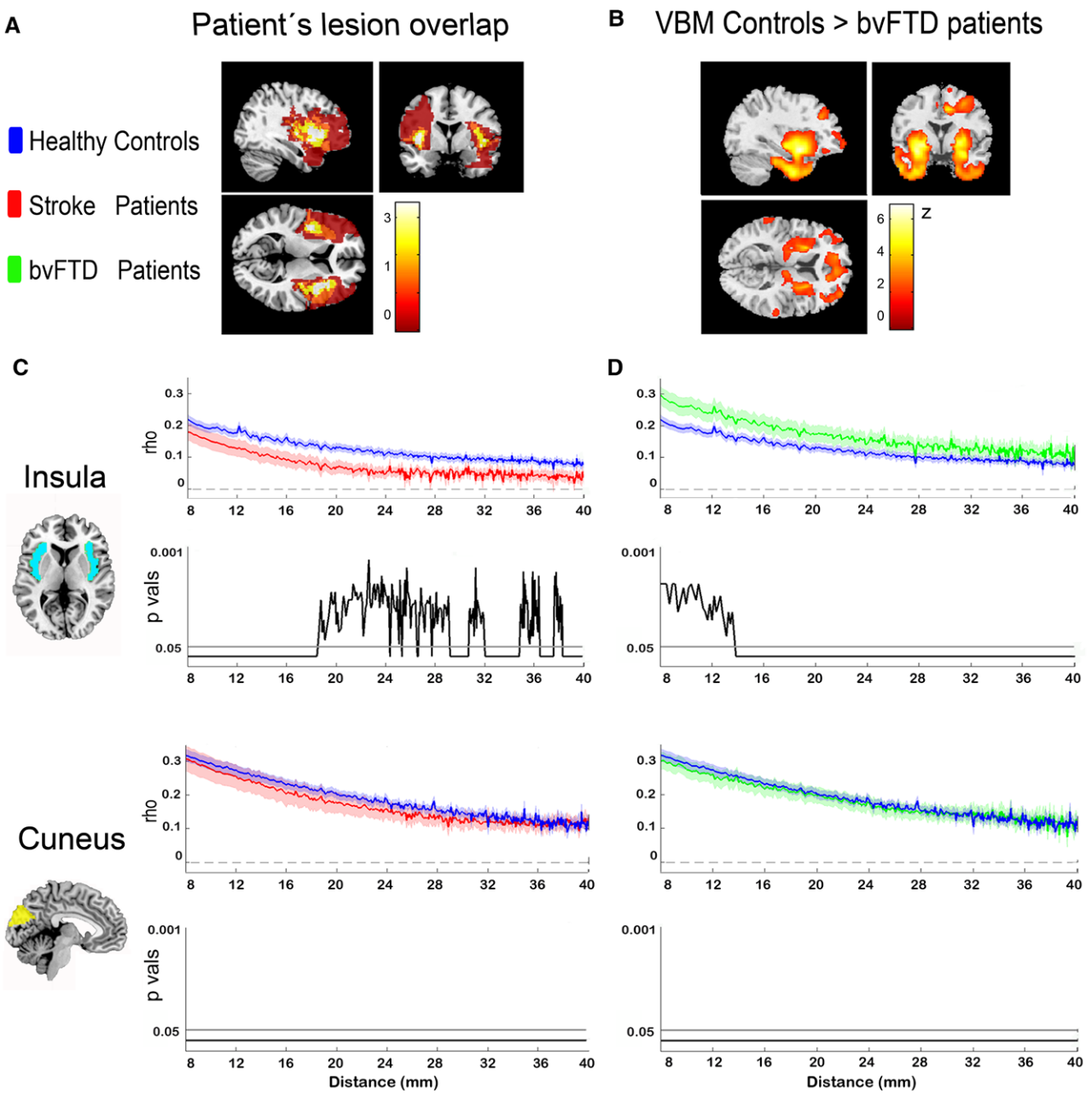

Figure. Functional connectivity of insular cortex in patients with stroke and behavioral variant frontotemporal dementia (bvFTD). **A**, Medial, coronal, and axial view of lesion overlap in patients with stroke (bar indicates the number patients). **B**, Atrophy of patients with bvFTD (voxel-based morphometry [VBM]) compared with controls, $P<0.05$, $\alpha=0.2$, false discovery rate corrected. Correlation function between voxels as a function of distance within the bilateral insular cortex (**top**) and the cuneus (**bottom**) for the stroke vs controls (**C**) and bvFTD vs controls (**D**). Charts showing the level of statistical significance between groups (*P* values) are presented under each graph.

hyperconnectivity between neighbor voxels in the same area ($P<0.05$, at a distance of ≈4–7 voxels or 11–14 mm; Figure D). Voxel-distance analyses of the cuneus revealed no significant differences among groups (Figure C and D).

Moreover, relative to participants with stroke, patients with bvFTD presented significant hyperconnectivity for all distances (from 4–20 voxels or 8 a 40 mm) in the InsC but not in the cuneus (Figure I in the online-only Data Supplement).

Analysis of global connectivity in patients with stroke relative to controls revealed hypoconnectivity in insulo-frontal hubs. Compared with controls, patients with bvFTD exhibited disconnection in salience-network hubs[4,8] (Section 2.3 and Figure II in the online-only Data Supplement).

Discussion

Each patient group exhibited a distinct pattern of connectivity decay as a function of neighboring-voxel distance in the InsC. Patients with stroke showed hypoconnectivity, as correlations decreased with increasing distance. Conversely, patients with bvFTD were characterized by hyperconnectivity, showing the opposite pattern of correlations. Lack

Table. Demographic Results

	Patients With Stroke	Patients With bvFTD	Healthy Controls	*P* Value
n (women/men)	8 (2/6)	11 (6/5)	14 (4/10)	0.30
Age*	M=55.62, SD=9.68 (38–66)	M=64.81, SD=5 (54–70)	M=57.21, SD=12.33 (33–72)	0.11
Formal education†	M=16.71, SD=4.65 (7–22)	M=14.45, SD=4.27 (4–19)	M=16.14, SD=2.90 (10–21)	0.42
WAT (premorbid IQ)	M=43.6, SD=2.89 (40–46)	M=40.2, SD=7.42 (25–49)	M=44.83, SD=4.91 (35–51)	0.23
MMSE	M=29, SD=1.41 (26–30)	M=25.11, SD=4.43 (18–30)	M=29.23, SD=1.42 (25–30)	0.003

IQ indicates intelligence quotient; M, mean; MMSE, Mini-Mental State Examination; and WAT, Word Accentuation Test.
*Age range.
†Time in years.

of differences in the cuneus, which proved intact in both diseases, suggests that local connectivity abnormalities are partly dependent on the underlying ischemic and neurodegenerative processes.

Regional connectivity has been successfully used to examine local connectivity patterns in healthy individuals.[12] Previous research has also shown increased and decreased long-range connections in patients with stroke.[7] Our study extends available findings by demonstrating that stroke induces abnormal local connectivity among distant InsC voxels (Figure C).

Studies about patients with bvFTD have revealed alterations in specific large-scale networks, manifested as both reduced and enhanced long-range connectivity.[8] Only one study assessing local connectivity in this pathology showed hyperconnectivity in the InsC and interpreted it as a compensatory response in bvFTD.[9] These findings align with our results, which showed that bvFTD, as opposed to stroke, features significant hyperconnectivity changes in nearby InsC voxels (Figure D).

Local hypoconnectivity in ischemic stroke could be the consequence of hypometabolism mediated by tissue hypoxia (eg, reduced adenosine triphosphate, mitochondrial damage, and release of DNA fragmentation proteins).[13] Conversely, hyperconnectivity in bvFTD can reflect the effect of protein aggregation and neurotoxicity,[4] which would activate compensatory mechanisms or disrupt the excitatory–inhibitory balance of damaged networks.[8,14]

Beyond these tentative explanations, our results suggest that topographically similar brain lesions with different causes may yield dissimilar aberrant changes in local connectivity. This highlights the importance of comparing diseases with different underlying mechanisms.[6] Importantly, our findings challenge the common assumption that damage to a given area results in similar connectivity disturbances irrespective of its causes. At the least, this evidence calls for a re-evaluation of current proposals that postulate that specific brain hubs may be similarly compromised by different pathological conditions.[15]

Our study has some limitations. Similar to previous studies,[9] our sample size was low. However, this limitation was considerably counteracted by the strict control of several relevant variables (eg, diagnosis, lesion cause, age, sex, intelligence quotient, education, and volume of insular affectation among patients with stroke and bvFTD). The detection of significant effects in target regions, and their absence in control areas, further attests to the adequacy of our samples.

Stroke damage is not restricted to the InsC. Nevertheless, all subjects had lesions exclusively caused by stroke and no comorbidity with other diseases. The main overlap among several compromised regions was found in the target region (InsC). Finally, images spatially normalized to allow for joint analysis of different pathological brains could provoke matching problems (especially in and around the stroke area). Yet, we largely minimized these negative effects of standard preprocessing by omitting spatial smoothing. This avoids shift of activation peaks and the reduction of spatial resolution.

Both patient groups evinced global hypoconnectivity, as previously reported separately for stroke[7] and neurodegeneration[9,10] (Section 3 and Figure II in the online-only Data Supplement). Nevertheless, global connectivity results should be taken with reserve. Extra-insular areas are not consistently damaged across patients with stroke and bvFTD. The InsC has widespread connections, and such diversity makes it difficult to find homogeneous samples warranting analysis of long-range connections. Thus, we cannot determine the extent to which deficits are associated with damage in the (1) InsC, (2) other areas, or (3) a combination of (1) and (2).

Previous reports supported the idea that different neural disorders with different causes involve similar disconnection patterns in characteristic brain hubs.[15] In contrast, we suggest that different causes and physiopathological processes may influence cerebral connectivity in dissimilar and specific ways. Such idiosyncratic patterns may reflect differences in molecular and temporal dynamics between cerebral ischemia and neurodegeneration.

Sources of Funding

This study was supported by grants from Fondo Nacional de Desarrollo Científico y Tecnológico Regular (FONDECYT Regular 1130920/1140114); Proyecto de investigación de Ciencia y Tecnología (PICT 2012-0412/2012-1309), Ineco Foundation, and Innovation and Dissemination Center for Neuromathematics (FAPESP Research #2013/07699-0, S.Paulo Research Foundation).

Disclosures

None.

References

1. van den Heuvel MP, Sporns O. Network hubs in the human brain. *Trends Cogn Sci*. 2013;17:683–696. doi: 10.1016/j.tics.2013.09.012.
2. Craig AD. How do you feel–now? The anterior insula and human awareness. *Nat Rev Neurosci*. 2009;10:59–70. doi: 10.1038/nrn2555.
3. Ibañez A, Gleichgerrcht E, Manes F. Clinical effects of insular damage in humans. *Brain Struct Funct*. 2010;214:397–410. doi: 10.1007/s00429-010-0256-y.

4. Seeley WW, Crawford RK, Zhou J, Miller BL, Greicius MD. Neurodegenerative diseases target large-scale human brain networks. *Neuron*. 2009;62:42–52. doi: 10.1016/j.neuron.2009.03.024.
5. Rascovsky K, Hodges JR, Knopman D, Mendez MF, Kramer JH, Neuhaus J, et al. Sensitivity of revised diagnostic criteria for the behavioural variant of frontotemporal dementia. *Brain*. 2011;134(Pt 9):2456–2477. doi: 10.1093/brain/awr179.
6. Baez S, Couto B, Torralva T, Sposato LA, Huepe D, Montañes P, et al. Comparing moral judgments of patients with frontotemporal dementia and frontal stroke. *JAMA Neurol*. 2014;71:1172–1176. doi: 10.1001/jamaneurol.2014.347.
7. Grefkes C, Fink GR. Connectivity-based approaches in stroke and recovery of function. *Lancet Neurol*. 2014;13:206–216. doi: 10.1016/S1474-4422(13)70264-3.
8. Pievani M, Filippini N, van den Heuvel MP, Cappa SF, Frisoni GB. Brain connectivity in neurodegenerative diseases–from phenotype to proteinopathy. *Nat Rev Neurol*. 2014;10:620–633. doi: 10.1038/nrneurol.2014.178.
9. Day GS, Farb NA, Tang-Wai DF, Masellis M, Black SE, Freedman M, et al. Salience network resting-state activity: prediction of frontotemporal dementia progression. *JAMA Neurol*. 2013;70:1249–1253. doi: 10.1001/jamaneurol.2013.3258.
10. Pasquini L, Scherr M, Tahmasian M, Meng C, Myers NE, Ortner M, et al. Link between hippocampus' raised local and eased global intrinsic connectivity in AD. *Alzheimers Dement*. 2015;11:475–484. doi: 10.1016/j.jalz.2014.02.007.
11. Zang Y, Jiang T, Lu Y, He Y, Tian L. Regional homogeneity approach to fMRI data analysis. *Neuroimage*. 2004;22:394–400. doi: 10.1016/j.neuroimage.2003.12.030.
12. Simmons WK, Avery JA, Barcalow JC, Bodurka J, Drevets WC, Bellgowan P. Keeping the body in mind: insula functional organization and functional connectivity integrate interoceptive, exteroceptive, and emotional awareness. *Hum Brain Mapp*. 2013;34:2944–2958. doi: 10.1002/hbm.22113.
13. Carmichael ST. Plasticity of cortical projections after stroke. *Neuroscientist*. 2003;9:64–75.
14. Ibañez A, Manes F. Contextual social cognition and the behavioral variant of frontotemporal dementia. *Neurology*. 2012;78:1354–1362. doi: 10.1212/WNL.0b013e3182518375.
15. Crossley NA, Mechelli A, Scott J, Carletti F, Fox PT, McGuire P, et al. The hubs of the human connectome are generally implicated in the anatomy of brain disorders. *Brain*. 2014;137(Pt 8):2382–2395. doi: 10.1093/brain/awu132.

SUPPLEMENTAL MATERIAL

Stroke and neurodegeneration induce different connectivity aberrations in the insula

1. Supplemental Methods

1.1. Participants

We recruited eight patients with chronic cerebrovascular lesions confined to insular structures. They also presented secondary damage in the putamen, the temporal poles, and frontal and parietal regions. These patients were assessed at least six months post-stroke in the Institute of Cognitive Neurology (INECO), Buenos Aires, Argentina. Their diagnoses were made by stroke specialists (See Table I for more details).

Additionally, 11 patients were selected following the revised criteria for probable bvFTD[1, 2]. The patients presented prominent changes in personality and social behavior, which were verified by their caregivers. All patients showed frontal atrophy on MRI, and frontal hypoperfusion on SPECT, when available. They were all in the early/mild stages of the disease and did not fulfill criteria for specific psychiatric disorders. They were diagnosed by bvFTD specialists.

All patients underwent a standard clinical examination that is necessary for accurate diagnosis and is part of a global institutional research project. This includes an extensive battery of neurological, neuropsychiatric, and neuropsychological assessments. In addition, a control group was formed with 14 healthy age- and education-matched participants. None of these subjects reported a history of psychiatric or neurological disease.

All participants were evaluated with the Word Accentuation Test (WAT)[3], which indexes premorbid IQ[4]; it consists of 51 low-frequency written Spanish words which lack orthographic accentuation. Participants are requested to read these words out loud with proper stress assignment, a task involving lexical knowledge. In addition, the Mini-Mental State Examination (MMSE) was administered to all groups as an overall measure of cognitive state[5].

1.2. MRI assessment and connectivity analysis

1.2.1. MRI acquisition

All participants were scanned in a 1.5 T Phillips Intera scanner with a standard head coil. A T1-weighted spin echo sequence was used to generate 120 contiguous axial slices (*TR* = 2300 ms; *TE* = 13 ms; flip angle = 68°; FOV = rectangular 256 mm; matrix size = 256 × 240 × 120; slice thickness = 1 mm) which covered all the brain surface and tissue.

For resting-state functional MRI (resting-fMRI), 33 (5-mm thick) axial slices were acquired parallel to the plane connecting the anterior and posterior commissures and covering the whole brain (TR = 2777 ms, TE = 50 ms, flip angle = 90). During fMRI acquisition, participants were instructed to think about their daily routines (e.g., the activities performed that day since waking or what they were going to do later that day). Additionally, they were requested to keep their eyes closed and to avoid moving and falling asleep.

1.2.2. Lesion mapping

Lesion masks were manually traced in native patient spaces according to visible damage on a T1 scan. All lesion masks were normalized to MNI space and then overlapped to obtain the lesion map.

1.2.3. Voxel-based morphometry

A voxel-based morphometry analysis was performed to account for global atrophy pattern in bvFTD patients. Data were preprocessed on the DARTEL Toolbox, following previously described procedures[6, 7].The images were segmented in grey matter, white matter, and cerebrospinal fluid volumes and then modulated. Next, 8 mm full-width half-maximum kernel images were smoothed, normalized to MNI space, and subjected to second-level analysis within general linear models on Statistical Parametric Mapping software (SPM8) (http://www.fil.ion.ucl.ac.uk/spm/software/spm8)[7]. A two-sample *t*-test between controls and the bvFTD group was performed and the results of this statistical parametric map were corrected for multiple comparisons (α= 0.2 FDR corrected; statistical significance was set at $p < .05$).

Additionally, global volumetric measures (grey matter, white matter, and cerebrospinal fluid) were calculated for bvFTD patients and controls via the *gets_total* script in Matlab. Structural T1 images were segmented with the segment tool of SPM8 to obtain grey matter, white matter, and cerebrospinal fluid maps. The script used these images to calculate the total volume of the three tissues, and their sum yielded the total intracranial volume.

To quantify the total "intact" insular grey matter in both patient groups, a grey matter map was obtained for each subject via the segment tool of SPM8. For stroke patients, a binary lesion mask was used to delimit the lesion and avoid mistaken voxel intensities. Then, "intact" grey matter volumes were calculated using the *gets_total* script in Matlab. To this end, we delimited the InsC ROI using the Automated Anatomical Labeling atlas[8] (AAL). To calculate the volume of infarcted/atrophied areas, we used the healthy subjects template (of grey matter in MNI space) generated in the segmentation step. The InsC ROI was superposed over this template to quantify the total grey matter volume of a "healthy" InsC. Thus, we calculated the volume of infarcted/atrophied grey matter in our patients by considering the whole volume of InsC and "intact" grey matter.

1.2.4. fMRI preprocessing

Functional images were tested on the Artifact Repair toolbox for SPM8 to improve fMRI analysis of high motion subjects[9]. This toolbox automatically detected noise in the raw data. Noisy volumes were deleted to avoid large outliers from propagating to valid data.

Functional images were then preprocessed on SPM8.Images were slice-time corrected, aligned to the mean volume of the session scanning, and normalized (using theSPM8 default echo-planar imaging template). To partially correct and remove low-frequency drifts from the MR scanner, we applied a band-pass filter between 0.01 and 0.05 Hz using the Resting-State fMRI Data Analysis Toolkit (REST, http://resting-fmri.sourceforge.net/[10]).

These frequencies lie in the range of slow frequency correlations of the resting networks[11]. Finally, applying these software tools, we regressed out six motion parameters estimated bySPM8. This last procedural step was performed to remove the potential variance introduced by spurious sources.

1.2.5. Long-range (global) connectivity analysis

All groups were compared in terms of long-range connectivity between InsC and other regions of interest (ROIs) –extracted from the AAL atlas[8]. Firstly, for between-ROI correlations, voxel time-series were averaged within each ROI. Functional connectivity was assessed in each subject by calculating Spearman's rank correlation coefficients in average time-series across ROIs, resulting in a 116 × 116 matrix for each subject. A *t*-test was performed to compare long-range functional connectivity in the InsC between groups. Classification data reported in Dosenbach et al.[12] were used to organize the ROIs. Nodes were arranged in six functionally defined networks: cingulo-opercular, sensorimotor, fronto-parietal, and occipital areas, as well as the default mode network and the cerebellum. After statistical analysis, we labeled the resulting nodes following Dosenbach's classification (Figure II).

1.2.6. Correlation function

Our aim was to study the interaction between brain voxels, namely, their correlation function[13]. In physics, a typical approach to describe an interaction system is to study how the interactions (measured, for example, by linear correlation) decay with increasing distance. In general, mutual dependence between two units of a system (in our case, voxels) decreases the further apart they are. The specific functional form of decay gives much information when the system is composed by identical units, as in homogeneous systems. In the case of the brain, this methodology can be useful to understand ranges of interaction and to distinguish different groups, as shown in this paper. The rationale is that if a brain region is affected by a disease, then their interactions should be modified.

BOLD temporal series and x-y-z coordinates in MNI space were calculated for each voxel in two bilateral regions of interest (ROIs): the bilateral insular cortex and cuneus (as defined in the Automated Anatomical Label atlas)[8].

We determined the degree of functional interaction between two voxels within these ROIs by calculating Spearman's rank correlation coefficients between both BOLD signals. This measure (henceforth, correlation function) was established in terms of the Euclidean distance (*d*) between voxels. This correlation function was calculated for each subject and ROI and averaged within groups[13]. Correlation functions between-group comparisons were made through the Montecarlo permutation test with bootstrap[14, 15]. This simple method offers a straightforward solution for multiple comparison problems and for data distribution assumptions[16]. The combined data from each group was randomly partitioned, and a *t*-test was calculated. This process was repeated 1. 000 times to construct the *t*-value distribution under the null hypothesis, which would be rejected by *t*-values greater than the most extreme 1% of the distribution (e.g., $p < .01$). This nonparametric permutation approach is considered comparable to statistical parametric mapping approach[16]. Also, Fisher z-transformation correlation functions for all comparisons are offered in the Figure III and IV.

1.2.7. Lesion-atrophy volume comparison

To control for possible differences among patient groups, we compared the volume of insular affectation by stroke or neurodegeneration. Lesion masks were superimposed over the bilateral insular ROI to extract the number of lesioned voxels within the IC. For the bvFTD group, segmented images from VBM analysis and this ROI were used to obtain the number of atrophied voxels within the insular cortex. A threshold of 0.2 was

established in order to discriminate between grey matter and whiter matter plus cerebrospinal fluid. A *t*-test was performed to compare the number of lesioned and atrophied voxels in the bilateral insula. No significant differences were obtained between the groups (p=.98). We performed another *t*-test to compare the volume of grey matter damage of bilateral InsC in each patient group. No significant differences were found (p = .94). Thus, both patient groups had a similar proportion of bilateral insular damage.

2. Extended Results

2.1. Damage areas from stroke patients

Table I. Regions (based on AAL) of damage areas in the stroke patients

Patient nº		1	2	3	4	5	6	7	8
Stroke etiology		I	I	I	I	I	H	I	I
AFFECTED REGIONS	Insula L								
	Putamen L								
	Temporal Sup L								
	Temporal Pole Sup L								
	Frontal InfTriangularis L								
	Frontal MidOrb L								
	Frontal Mid L								
	Frontal Sup Orb L								
	Frontal Sup L								
	Frontal Sup Orb L								
	Heschl L								
	Roldanic Operculum L								
	Insula R								
	Putamen R								
	Temporal Sup R								
	Temporal Pole Sup R								
	Frontal Inf Orb R								
	Frontal InfTriangularisR								
	Frontal InfOperculum R								
	Frontal Mid R								
	Frontal Mid Orb R								
	Roldanic Operculum R								
	Supramarginal R								

I: Ischemic stroke; H: Hemorrhagic stroke; L: left; R: right, Sup: superior, Inf: inferior, Orb: orbital; AAL: Automated Anatomical Labeling Atlas; Pink: patients with left damage; Green: patients with right damage

2.2. Voxel-based morphometry

Voxel-based morphometry of the bvFTD group revealed a pattern of global atrophy in the IC, as well as frontal and temporal lobe structures, as reported in previous studies[17, 18]($p < .05$, α= 0.2 FDR corrected). Table II specifies all atrophied regions that were significantly different from their counterparts in the control group and in Table III we

provided the global volumetric measures. Grey matter volume of intact/infarcted/atrophied InsC for both patient groups is described in Tables IV and V.

Table II. Regions (based on AAL) of significant atrophy (local maxima) in bvFTD patients compared with healthy controls

Region	X	Y	Z	Peak t	Peak z
Insula	-36	0.73	-12	6.77	4.97
Palladium L	-22.5	-6	-4.5	6.10	4.66
Palladium R	19.5	4.5	-6	5.57	4.38
Amygdala R	24	-6	-13.5	5.62	4.42
Fusiform L	-36	-4.5	-40.5	5.61	4.41
Thalamus L	-15	-10.5	-3	4.10	3.51
Thalamus R	16.5	-9	-3	5.49	4.34
Cingulum R	10.5	19.5	42	5.33	4.26
Frontal Superior L	-13.5	49.5	39	3.90	3.38
Frontal Superior R	13.5	33	42	4.76	3.93
Frontal Mid Superior L	-7.5	27	58.5	5.15	4.16
Frontal Mid Superior R	7.5	27	48	5.09	4.13
Frontal Mid Superior R	30	36	28.5	4.25	3.62
Temporal Inferior L	-43.5	9	-37.5	5.30	4.24
Temporal Inferior R	-51	3	-34.5	4.62	3.85
Temporal Pole Mid R	39	7.5	-37.5	4.40	3.71
Supplementary motor area R	10.5	12	45	5.18	4.18

All $p<0.05$ $\alpha= 0.2$ FDR corrected); AAL: Automated Anatomical Labeling Atlas; L: left; R: right

Table III. Global volumetric measures

Subjects	GM	WM	CSF	TIV
Healthy controls	*M*=686.50, *SD*=52.23 (604.90-793.72)	*M*=536.46, *SD*=51 (475.93-607.74)	*M*=314.58, *SD*=27.94 (350.56-273.92)	*M*=1537.54, *SD*=118.40 (1375.78-1732.22)
Percentage[#]	*M*=44.66, *SD*=0.90	*M*=34.86, *SD*=1.23	*M*=20.47, *SD*=1.20	-
bvFTD patients	*M*=659.78, *SD*=57.48 (597.53-772.38)	*M*=514.11, *SD*=43.70(445.12-571.62)	*M*=334.47, *SD*=37.34 (281.61-391.90)	*M*=1508.36, *SD*=129.68 (1397.03-1735.90)
Percentage[#]	*M*=43.75, *SD*=0.93	*M*=34.02, *SD*=1.04	*M*=22.15, *SD*=1.24	-

All volumes are in ml. GM: grey matter; WM: white matter; CSF: cerebrospinal fluid; TIV: total intracranial volume; *M*: mean; *SD*: standard deviation; (): range; [#] Percentage (%) relative to TIV.

Table IV. Insular grey matter volume for stroke patients

	Left InsC		Right InsC	
Patient n°	**Intact GM volume**	**Infarcted tissue volume**	**Intact GM volume**	**Infarcted tissue volume**
1 L	4.95	2.09	5.85	-
2 L	3.07	3.97	5.40	-
3 L	4.73	2.31	5.65	-
4 R	7.31	-	3.21	3.95
5 R	5.75	-	4.45	2.71
6 R	5.90	-	5.21	1.95
7 R	7.55	-	4.31	2.85
8 R	7.21	-	5.84	1.32

All volumes are in ml. L: left insular stroke patient; R: right insular stoke patient.

Table V. Insular grey matter volume for bvFTD patients

	Left InsC		Right InsC	
Patient n°	**Intact GM volume**	**Atrophied tissue volume**	**Intact GM volume**	**Atrophied tissue volume**
1	4.93	2.11	4.62	2.54
2	4.41	2.63	3.21	3.95
3	4.68	2.36	3.40	3.76
4	4.93	2.11	2.88	4.28
5	5.05	1.99	4.00	3.16
6	4.70	2.34	4.89	2.27
7	5.78	1.26	5.58	1.58
8	4.81	2.23	4.77	2.39
9	5.88	1.16	5.79	1.37
10	1.27	5.77	2.10	5.06
11	4.86	2.18	4.76	2.40

All volumes are in ml.

2.3. Insular long-range (global) connectivity

Analysis of long-range connections in stroke patients relative to controls revealed hypoconnectivity in insulo-frontal hubs (FDR corrected, $p < .05$). The left InsC was significantly disconnected from the right medial region of the superior frontal gyrus (FDR corrected, $p < .01$). The right InsC was also significantly disconnected from the left inferior frontal gyrus (FDR corrected, $p < .01$) and the right gyrus rectus (FDR corrected, $p < .01$). Instead, relative to controls, bvFTD patients showed reduced connectivity with the salience-network hubs[18, 19] (FDR corrected, $p < .05$). The left InsC showed disconnection from the right InsC (FDR corrected, $p < .01$), the right thalamus (FDR corrected, $p < .01$), and the left triangularis part of the inferior frontal gyrus (FDR corrected, $p < .01$). The right InsC exhibited reduced connectivity with the left medial region of the superior frontal gyrus (FDR corrected, $p < .01$), the left orbital region of

the superior frontal gyrus (FDR corrected, $p < .01$), and the left precentral gyrus (FDR corrected, $p < .01$) (Figure II).

3. Supplemental Discussion

Relative to controls, both patient groups presented long-range hypoconnectivity. Salience network areas were expectedly compromised in bvFTD[18-21], whereas frontal areas were disturbed in stroke patients.

Our main results in bvFTD align with the finding that Alzheimer's disease involves local hyperconnectivity in the hippocampus and global hypoconnectivity between the hippocampus and other regions associated with the default mode network[22]. However, diversity of damage across patients makes it difficult to find homogeneous samples warranting analysis of long-range connections. In most stroke patients, insular damage extended to other areas (Figure 1. A). The same was true of bvFTD atrophy. Thus, long-range connectivity results must be interpreted with caution.

4. Supplemental figures

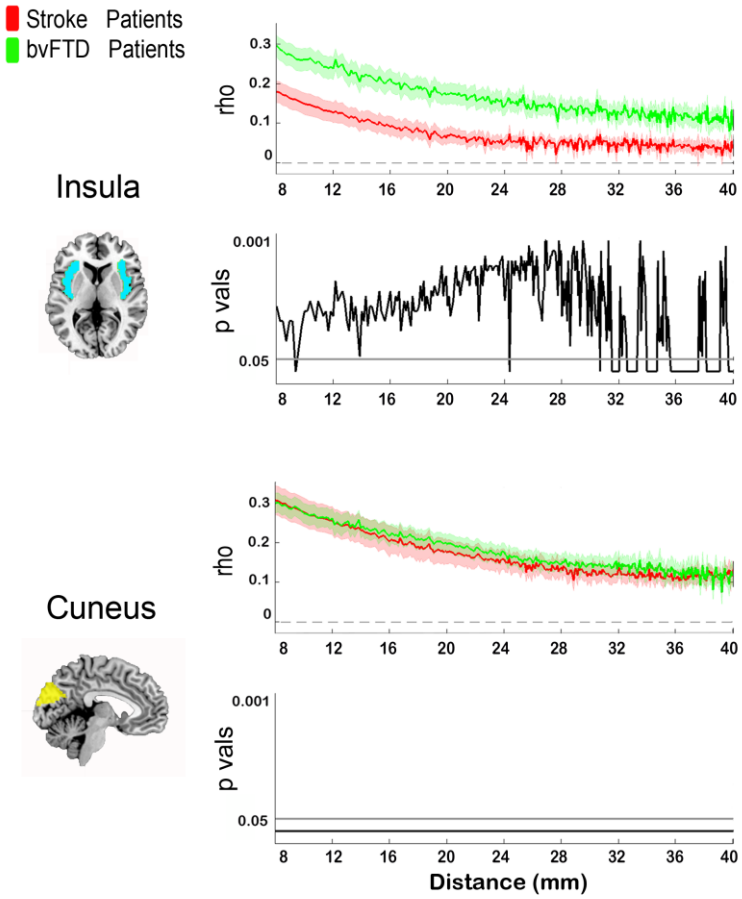

Figure I. Pairwise Spearman's rank correlations between voxels as a function of distance within the bilateral insular cortex (top) and the cuneus (bottom) for the stroke and bvFTD groups. Charts showing the level of statistical significance between groups (*p* values) are presented under each graph.

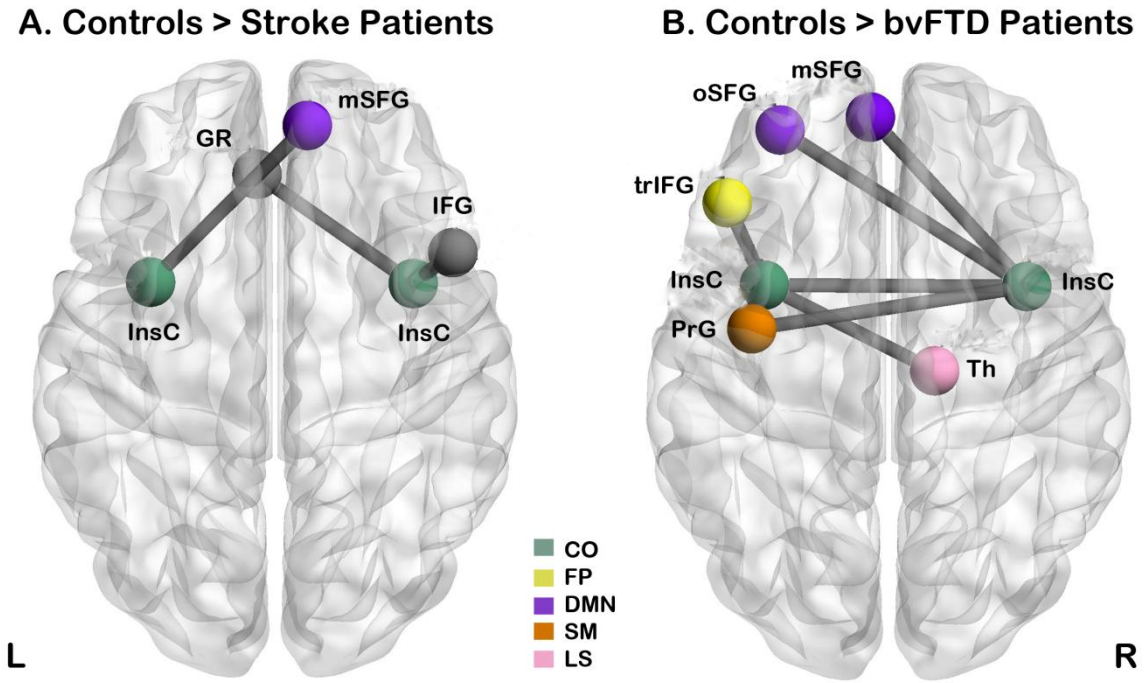

Figure II: long-range (global) InsC functional connectivity in stroke patients and bvFTD in comparison to controls. Comparisons of insular long-range functional connectivity between groups considering ROIs extracted from the AAL atlas. ROIs are labeled following[12]. A. Functionally disconnected regions for stroke patients in comparison to controls (FDR corrected, statistical significance set at $p < .05$). B: Functionally disconnected regions for bvFTD patients in comparison to controls (FDR corrected, statistical significance set at $p < .05$). Regions: InsC: insular cortex; GR: gyrus rectus; mSFG: medial region of the superior frontal gyrus; IFG: inferior frontal gyrus; PrG: precentral gyrus; tfIFG: triangularis part of the inferior frontal gyrus; oSFG: orbital region of the superior frontal gyrus; Th: thalamus. Networks: CO: cingulo-opercular; FP: fronto-parietal; DMN: default mode network; SM: sensorimotor; LS: limbic system (grey nodes do not belong to any functional network). Hemispheres: L: left; R: right. ROIs: regions of interest. AAL: Automated Anatomical Labeling.

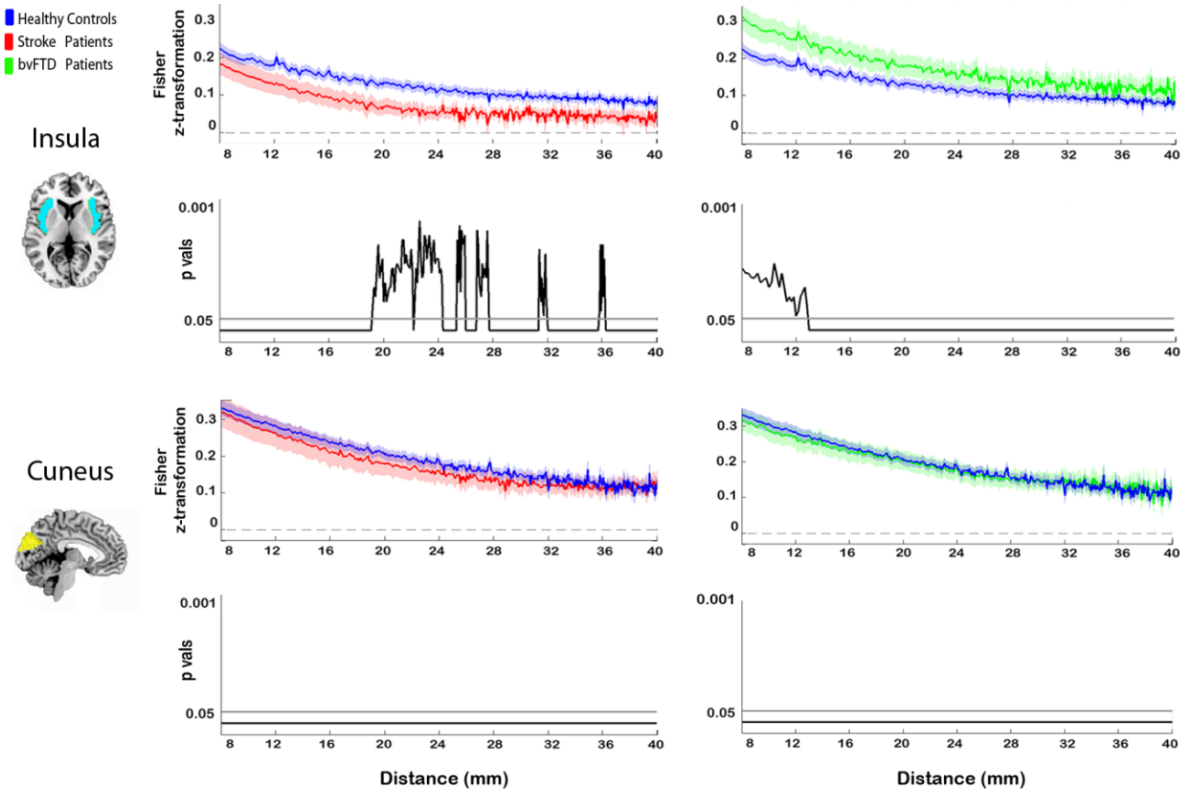

Figure III: Fisher z-transformation of correlations between voxels as a function of distance within the bilateral insular cortex (top) and the cuneus (bottom), for stroke vs. controls and bvFTD vs. controls.

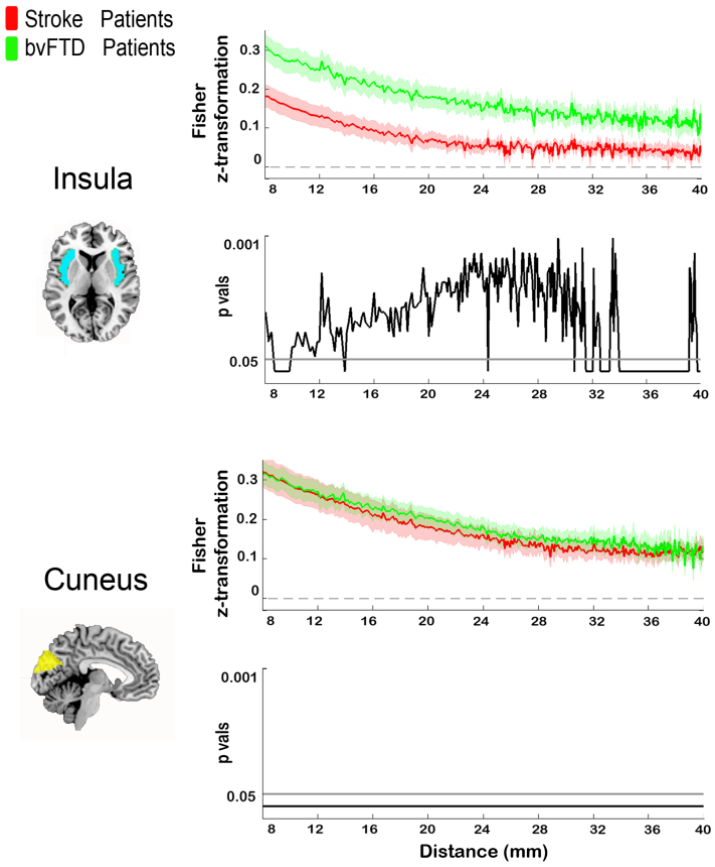

Figure IV: Fisher z-transformation of correlations between voxels as a function of distance within the bilateral insular cortex (top) and the cuneus (bottom), for stroke vs. bvFTD.

5. Supplemental references

1. Rascovsky K, Hodges JR, Knopman D, Mendez MF, Kramer JH, Neuhaus J, et al. Sensitivity of revised diagnostic criteria for the behavioural variant of frontotemporal dementia. *Brain : a journal of neurology*. 2011;134:2456-2477
2. Neary D, Snowden JS, Gustafson L, Passant U, Stuss D, Black S, et al. Frontotemporal lobar degeneration: A consensus on clinical diagnostic criteria. *Neurology*. 1998;51:1546-1554
3. Burin DI, Jorge RE, Arizaga RA, Paulsen JS. Estimation of premorbid intelligence: The word accentuation test-- buenos aires version. *J Clin Exp Neuropsychol*. 2000;22:677-685
4. Torralva T, Roca M, Gleichgerrcht E, Lopez P, Manes F. Ineco frontal screening (ifs): A brief, sensitive, and specific tool to assess executive functions in dementia. *J Int Neuropsychol Soc*. 2009;15:777-786
5. Butman J, Allegri RF, Harris P, Drake M. [spanish verbal fluency. Normative data in argentina]. *Medicina*. 2000;60:561-564
6. Ashburner J, Friston KJ. Voxel-based morphometry--the methods. *Neuroimage*. 2000;11:805-821
7. Couto B, Manes F, Montanes P, Matallana D, Reyes P, Velasquez M, et al. Structural neuroimaging of social cognition in progressive non-fluent aphasia and behavioral variant of frontotemporal dementia. *Frontiers in human neuroscience*. 2013;7:467
8. Tzourio-Mazoyer N, Landeau B, Papathanassiou D, Crivello F, Etard O, Delcroix N, et al. Automated anatomical labeling of activations in spm using a macroscopic anatomical parcellation of the mni mri single-subject brain. *NeuroImage*. 2002;15:273-289
9. Singh MK, Chang KD, Mazaika P, Garrett A, Adleman N, Kelley R, et al. Neural correlates of response inhibition in pediatric bipolar disorder. *Journal of child and adolescent psychopharmacology*. 2010;20:15-24
10. Song XW, Dong ZY, Long XY, Li SF, Zuo XN, Zhu CZ, et al. Rest: A toolkit for resting-state functional magnetic resonance imaging data processing. *PloS one*. 2011;6:e25031
11. Fox MD, Snyder AZ, Vincent JL, Corbetta M, Van Essen DC, Raichle ME. The human brain is intrinsically organized into dynamic, anticorrelated functional networks. *Proceedings of the National Academy of Sciences of the United States of America*. 2005;102:9673-9678
12. Dosenbach NU, Nardos B, Cohen AL, Fair DA, Power JD, Church JA, et al. Prediction of individual brain maturity using fmri. *Science*. 2010;329:1358-1361
13. Fraiman D, Chialvo DR. What kind of noise is brain noise: Anomalous scaling behavior of the resting brain activity fluctuations. *Frontiers in physiology*. 2012;3:307
14. Ibanez A, Cardona JF, Dos Santos YV, Blenkmann A, Aravena P, Roca M, et al. Motor-language coupling: Direct evidence from early parkinson's disease and

intracranial cortical recordings. *Cortex; a journal devoted to the study of the nervous system and behavior*. 2013;49:968-984
15. Manly BFJ. *Randomization, bootstrap and monte carlo methods in biology*. Chapman & Hall/ CRC; 1997.
16. Nichols TE, Holmes AP. Nonparametric permutation tests for functional neuroimaging: A primer with examples. *Human brain mapping*. 2002;15:1-25
17. Rankin KP, Gorno-Tempini ML, Allison SC, Stanley CM, Glenn S, Weiner MW, et al. Structural anatomy of empathy in neurodegenerative disease. *Brain : a journal of neurology*. 2006;129:2945-2956
18. Seeley WW, Crawford RK, Zhou J, Miller BL, Greicius MD. Neurodegenerative diseases target large-scale human brain networks. *Neuron*. 2009;62:42-52
19. Pievani M, de Haan W, Wu T, Seeley WW, Frisoni GB. Functional network disruption in the degenerative dementias. *The Lancet. Neurology*. 2011;10:829-843
20. Pievani M, Filippini N, van den Heuvel MP, Cappa SF, Frisoni GB. Brain connectivity in neurodegenerative diseases--from phenotype to proteinopathy. *Nature reviews. Neurology*. 2014;10:620-633
21. Zhou J, Seeley WW. Network dysfunction in alzheimer's disease and frontotemporal dementia: Implications for psychiatry. *Biological psychiatry*. 2014;75:565-573
22. Pasquini L, Scherr M, Tahmasian M, Meng C, Myers NE, Ortner M, et al. Link between hippocampus' raised local and eased global intrinsic connectivity in ad. *Alzheimer's & dementia : the journal of the Alzheimer's Association*. 2015;11:475-484

Stroke and Neurodegeneration Induce Different Connectivity Aberrations in the Insula

Indira García-Cordero, Lucas Sedeño, Daniel Fraiman, Damian Craiem, Laura Alethia de la Fuente, Paula Salamone, Cecilia Serrano, Luciano Sposato, Facundo Manes and Agustín Ibañez

Stroke. published online July 16, 2015;
Stroke is published by the American Heart Association, 7272 Greenville Avenue, Dallas, TX 75231

Print ISSN: 0039-2499. Online ISSN: 1524-4628